LAWRENCE
LIVERMORE
NATIONAL
LABORATORY

UCRL-PROC-208242

Crevice Corrosion Susceptibility of Alloy 22 in Fluoride and Chloride Containing Solutions

S. Daniel Day, Raúl B. Rebak

November 30, 2004

CORROSION/2005, Conference and Exposition
Houston, TX, United States
April 3, 2005 through April 7, 2005

10 November 2004
Paper 05599 prepared to be presented during the CORROSION/2005 Conference, 3-7 April 2005 in Houston, TX

CREVICE CORROSION SUSCEPTIBILITY OF ALLOY 22 IN FLUORIDE AND CHLORIDE CONTAINING ENVIRONMENTS

Martín A. Rodríguez and Ricardo M. Carranza
Departamento de Materiales, Comisión Nacional de Energía Atómica
Av. Gral. Paz 1499
B1650KNA San Martín, Buenos Aires, ARGENTINA

S. Daniel Day and Raúl B. Rebak
Lawrence Livermore National Laboratory
7000 East Ave, L-631
Livermore, CA 94550, USA

ABSTRACT

Alloy 22 (N06022) is highly resistant to crevice corrosion in pure chloride (Cl^-) solutions. Little research has been conducted to explore the resistance of this alloy to other halides such as fluoride (F^-) and bromide (Br^-). Even less information is available exploring the behavior of localized corrosion for Alloy 22 in mixtures of the halide ions. Standard electrochemical tests such as polarization resistance and cyclic potentiodynamic polarization (CPP), were conducted to explore the resistance to corrosion of Alloy 22 in deaerated aqueous solutions of 1 M NaCl, 1 M NaF and 0.5 M NaCl + 0.5 M NaF solutions at 60°C and 90°C. Results show that the general corrosion rate was the lowest in the mixed halide solution and the highest in the pure chloride solution. Alloy 22 was not susceptible to localized corrosion in the pure fluoride solution. In 1 M NaCl solution, Alloy 22 was susceptible to crevice corrosion at 90°C. In the mixed halide solution Alloy 22 was susceptible to crevice corrosion both at 60°C and 90°C.

Keywords: N06022, chloride, fluoride, temperature, corrosion rate, crevice corrosion

INTRODUCTION

Alloy 22 (N06022) is nickel (Ni) based and contains nominally 22% Chromium (Cr), 13% Molybdenum (Mo) and 3% tungsten (W). [1] Alloy 22 belongs to the Ni-Cr-Mo family of nickel based alloys, which also include alloys such as C-4 (N06455), C-276 (N10276), C-2000 (N06200), 59 (N06059) and 686 (N06686). [1] The Ni-Cr-Mo alloys were designed to withstand the most aggressive industrial applications, including reducing acids such as hydrochloric and oxidizing acids such as nitric. Chromium is

the beneficial alloying element added for protection against oxidizing conditions and molybdenum is the beneficial alloying element to protect against reducing conditions. [2-4] The base element (nickel) protects the alloy against caustic conditions. [2-4] All three elements, Ni, Cr and Mo act synergistically to provide resistance to environmentally assisted cracking in hot concentrated chloride solutions. [2-4] The alloying elements Cr and Mo also provide resistance to localized corrosion such as pitting and crevice corrosion in chloride containing solutions. Some of the Ni-Cr-Mo alloys also contain a small amount of tungsten (W), which may act in a similar way as Mo regarding protection against localized corrosion. [5] Ni-Cr-Mo alloys are practically immune to pitting corrosion but they may suffer crevice corrosion under aggressive environmental conditions.

FACTORS INFLUENCING CREVICE CORROSION OF ALLOY 22

Many times, for an alloy selection process in an industrial application, the pitting equivalent ratio (PRE) is applied to Ni-Cr-Mo alloys (and stainless steels). [5-7] The higher the PRE the higher the resistance of the alloy to localized corrosion. Alloy 22 has one of the highest PRE numbers for nickel based alloys and therefore is one of the most resistant engineering alloys to localized corrosion. [3,5,8] For example, Alloy 22 has been in service for over ten years in a flue-gas desulfurization (FGD) plant in the United Kingdom without suffering localized corrosion. [9] Due to its excellent resistance to general and localized corrosion, Alloy 22 was selected for the fabrication of the outer shell of the high level nuclear waste containers for the proposed Yucca Mountain repository. [10-11]

For practical purposes, Alloy 22 can be considered not susceptible to pitting corrosion in chloride containing environments. However, Alloy 22 may be prone to crevice corrosion in some conditions. [12-14] There are many factors influencing the susceptibility of Alloy 22 to suffer crevice corrosion. These factors can be classified into environmental or external factors and metallurgical or internal factors. The external factors include:

a. Chloride concentration
b. Temperature
c. Applied potential
d. Presence of inhibitors such as nitrate, sulfate and carbonate
e. Presence of other deleterious species such as fluoride and bromide
f. Proton activity (pH)
g. Crevice former geometry (tightness of the crevice)
h. Type of crevicing material, etc.

Internal factors are related to the metallurgical condition of Alloy 22, that is, for example,

1. Is the alloy in the mill-annealed (MA) wrought condition?
2. Is there a weld seam containing a cast or dendritic microstructure?
3. Was the alloy solution heat-treated?
4. Is there a solution annealing plus water quenching oxide film on the surface?
5. Was the material thermally aged? At what time and temperature?
6. Are there secondary phases precipitated? Etc.

Each one of these factors, external and internal affect the susceptibility of Alloy 22 to crevice corrosion in a certain way, considering that all the other factors remain unchanged. There are many publications discussing some of the factors mentioned above. [12-29] Only the effect of halides other than chloride will be briefly discussed in this paper.

Effect of fluoride and bromide

The effect of fluoride (F^-) and bromide (Br^-) ions on the corrosion behavior of Alloy 22 has not been as extensively investigated as the effect of chloride (Cl^-) ions was. Prismatic Alloy 22 specimens (ASTM G 5) were tested in 1 M NaCl pH 6 and in 1 M NaF pH 9 solutions at 50°C. [25] The passive current density in both solutions was the same and approximately 2 x 10^{-6} A/cm². The breakdown potential (E20) was 635 mV SCE in the chloride solution and 344 mV SCE in the fluoride solution. The difference in the breakdown potential can be mainly attributed to a difference in the pH of the electrolytes. The reversed CPP did not show hysteresis in either solution and the specimens did not suffer either pitting corrosion or crevice corrosion in any of these electrolytes, even after polarization to potentials higher than 800 mV. [25] Dunn et al. tested the influence of fluoride ions when added to 0.5 M NaCl solutions at 95°C for 5 min at 870°C thermally aged Alloy 22. [22] They reported that fluoride anion was not an inhibitor to crevice corrosion as found for nitrate, sulfate and carbonate oxyanions. [22-23]

Rodríguez et al. tested the corrosion susceptibility of MA and thermally aged Alloy 22 in 1 M NaF solutions at pH 6, 7.3 and 9. [26] Thermal aging was performed to create conditions of full aging with TCP phases (10 h at 760°C) and long range ordering (LRO or 1000 h at 538°C). Rodríguez et al. did not find localized corrosion (pttting or crevice corrosion) in any of the tested conditions even though the specimens were polarized to anodic potentials where current densities of up to 10 mA/cm² were applied. Small hystereses observed in the reverse CPP were attributed to uniform film dissolution in the metal. [26] Rodríguez et al. also performed electrochemical tests for Alloy 22 under the same metallurgical conditions in 1 M NaCl pH 2, 6 and 9 and 0.5 M NaCl + 0.5 M NaF at pH 6 and 9. [27] Comparing their results with the 1 M NaF results they concluded that Alloy 22 seemed more susceptible to crevice corrosion in the mixed salt solution than in the pure 1 M NaCl solution of the same pH. [27]

Limited studies exist on the effect of bromide ions on the localized corrosion susceptibility of Alloy 22. Cyclic potentiodynamic polarization (CPP) tests were carried out in 1 M NaCl and 1 M NaBr solutions at 50°C. [28] Both solutions had a similar pH of approximately 6. A slightly higher repassivation potential was reported for MA Alloy 22 in the bromide solution than in the chloride solution. However, under the tested conditions Alloy 22 did not suffer either crevice or pitting corrosion in neither solution. [28] It has been reported that alloying elements such as Mo, which are highly beneficial for protection against localized corrosion in chloride solutions may not be as efficient in bromide containing solutions. [28]

The purpose of the current research was to explore the behavior of Alloy 22 in 1 M NaCl, 1 M NaF and 0.5 M NaCl + 0.5 M NaF at 60°C and 90°C. Results on corrosion potential (E_{corr}), polarization resistance, and localized corrosion resistance are presented.

EXPERIMENTAL

Alloy 22 (N06022) specimens were prepared from 1-inch thick commercial plates. The chemical compositions are given in Table 1. All the tested material was wrought mill annealed (MA). The specimens were multiple crevice assemblies (MCA) or lollipops, which were fabricated based on the washer for crevice forming described in ASTM G 48. [30] The MCA specimen has been described before. [13,17,19] Two specimens were PCA or prism crevice assembly. [14] The tested surface areas were approximately 11 cm² for the MCA and 14 cm² for the PCA specimens. The MCA specimens were partially immersed in the electrolyte to a 2-inch depth and the PCA specimens were fully immersed. Both MCA and PCA had the same crevicing mechanism. All the tested specimens had a finished grinding of abrasive paper number 600 and were degreased in acetone and treated ultrasonically for 5 minutes in de-ionized (DI) water 1 hour prior to testing.

Electrochemical tests were carried out in deaerated 1 M sodium halide solutions at 60°C and 90°C. These included: 1 M sodium chloride (NaCl), 1 M sodium fluoride (NaF) and 0.5 M NaCl + 0.5 M NaF. The pH of these solutions was approximately 6 for NaCl, 9 for NaF and 8 for the mixed salt solution. Nitrogen (N_2) was purged through the solution at a flow rate of 100cc/min for 24 hours while the corrosion potential (E_{corr}) was monitored. Nitrogen bubbling was continued throughout all the electrochemical tests. The electrochemical tests were conducted in a one-liter, three-electrode, borosilicate glass flask (ASTM G 5). [30] A water-cooled condenser combined with a water trap was used to avoid evaporation of the solution and to prevent the ingress of air (oxygen). The temperature of the solution was controlled by immersing the cell in a thermostatisized silicone oil bath, which was kept at a constant temperature. All the tests were carried out at ambient pressure. The reference electrode was saturated silver chloride (SSC) electrode, which has a potential of 199 mV more positive than the standard hydrogen electrode (SHE). The reference electrode was connected to the solution through a water-jacketed Luggin probe so that the electrode was maintained at near ambient temperature. The counter electrode was a flag (36 cm^2) of platinum foil spot-welded to a platinum wire. All the potentials in this paper are reported in the SSC scale.

Basically the test sequence for each specimen consisted of three parts: (1) E_{corr} evolution as a function of time for 24 h, (2) Polarization Resistance (ASTM G 59) [30] three subsequent times and (3) Cyclic Potentiodynamic Polarization (CPP) (ASTM G 61). [30]

Polarization Resistance (ASTM G 59): Corrosion rates (CR) were obtained using the polarization resistance method (ASTM G 59). Each one of these tests lasts approximately four minutes. An initial potential of 20 mV below the corrosion potential (E_{corr}) was ramped to a final potential of 20 mV above E_{corr} at a rate of 0.167 mV/s. Linear fits were constrained to the potential range of 10 mV below E_{corr} to 10 mV above E_{corr} putting the potential (independent variable) in the X-axis. The linear fit produces a value of slope which is the resistance to polarization R_p. The Tafel constants, b_a and b_c, were assumed to be $\pm$ 0.12 V/decade. Corrosion rates were calculated using Equation 1

$$i_{corr} = \frac{1}{R_p} \cdot \frac{b_a \cdot b_c}{2.303(b_a + b_c)} \ldots and \cdots CR(\mu m / yr) = k \frac{i_{corr}}{\rho} EW \qquad \textbf{(1)}$$

Where k is a conversion factor, i_{corr} is the calculated corrosion current density in A/cm^2 (using values of the slope R_p in V/A), EW is the equivalent weight, and ρ is the density of Alloy 22 (8.69 g/cm^3). Assuming an equivalent dissolution of the major alloying elements as Ni^{2+}, Cr^{3+}, Mo^{6+}, Fe^{2+}, and W^{6+}, the EW for Alloy 22 is 23.28 (ASTM G 102). [30]

Cyclic Potentiodynamic Polarization - CPP (ASTM G 61): The cyclic potentiodynamic polarization technique, CPP (ASTM G 61) id one of the tests commonly used to assess the susceptibility of Alloy 22 to localized corrosion and its passive stability. The potential scan was started 150 mV below E_{corr} at a set scan rate of 0.167 mV/s. The scan direction was reversed when the current density reached 5 mA/cm^2 in the forward scan. Depending on the range of applied potentials, each CPP test could last between 1 h and 3 h. After the CPP tests, the specimens were examined in an optical stereomicroscope at a magnification of at least 20 times to establish the mode and location of the attack.

RESULTS AND DISCUSSION

The Corrosion Potential (E_{corr})

Figures 1-3 show the evolution of the corrosion potential (E_{corr}) of individual MCA specimens of Alloy 22 at 60°C and 90°C in 1 M NaCl, 1 M NaF and 0.5 M NaCl + 0.5 M NaF, respectively. In the

three halide-environments, the evolution of E_{corr} to the final values was faster at 90°C than at 60°C and at the end of the 24-h immersion time, the E_{corr} was higher at 60°C than at 90°C. The findings are reasonable since the kinetics of electrode processes are expected to be faster and the alloy be more active at the higher temperature. Figure 4 shows the evolution of E_{corr} for the three solutions at 90°C. In the pure salt solutions, E_{corr} was lower in presence of NaF probably because the pH of this solution was higher that that of the NaCl solution. However, the behavior in the mixed salt solution (pH ~ 8) did not follow the pH effect trend and exhibited the highest E_{corr} value. The value of E_{corr} in the mixed solution suggests that fluoride ions seem to inhibit the general corrosion process of Alloy 22 when present with chloride ions. The same trend in E_{corr} of Figure 4 for 24-h immersion times was also observed at 60°C (Table 2). The values of E_{corr} in Table 2 are 24-h values and may not be the final steady-state values of the alloy in the reported environments. It has been reported before that the average value of E_{corr} of four rod-specimens immersed in an aerated solution of 1 M NaF at 90°C for more than four months was -111 ± 3 mV SSC. [31]

Polarization Resistance (R_p) and Corrosion Rate (CR)

Figures 5-6 show the resistance to polarization of individual Alloy 22 specimens in the three electrolyte solutions at 60°C and 90°C, respectively. At both temperatures, the highest resistance to polarization corresponded to the mixed halide solution and the lowest to the NaF solution. This is in agreement with the alloy activity according to the values of E_{corr} (Figure 4). Table 2 shows the corrosion rates for the individual specimens for all the tested conditions, which were calculated from resistance to polarization slopes (similar to Figures 5-6) using Equation 1. Figure 7 shows the average corrosion rates at both temperatures. At 60°C, the average corrosion rate of Alloy 22 in the three electrolytes was generally below 0.5 µm/year. The lowest corrosion rate was for the mixed halide solution at 0.28 µm/year. At 90°C, the highest corrosion rate was for the NaF solution at 2.1 µm/year and the lowest for the mixed halide solution at 0.55 µm/year. In all the tested electrolytes, the corrosion rate increased as the temperature increased. The values of corrosion rate (or resistance to polarization) in Table 2 and Figures 5-7 suggest that fluoride ions may act as an inhibitor for general corrosion of Alloy 22 in chloride solutions. On the other hand, at 90°C, the highest corrosion rate was obtained in pure fluoride solutions.

Cyclic Potentiodynamic Polarizations (CPP)

Figures 8-10 show the cyclic potentiodynamic polarization curves for individual Alloy 22 specimens in deaerated solutions at 60°C and 90°C of 1 M NaCl, 1 M NaF and 0.5 M NaCl + 0.5 M NaF, respectively. Figure 8 shows that in the 1 M NaCl solution, both curves had an anodic peak in the passive region of potentials. At 60°C the anodic peak occurred at approximately –110 mV SSC and at 90°C the anodic peak occurred at a lower potential, or approximately –160 mV SSC. The origin is these anodic peaks is not fully understood. They are pH and temperature dependent and seem to be associated with further oxidation of metal species (such as Mo and Ni) in the oxide film. The breakdown potential was lower at the higher temperature (see also Table 2). During the reverse scan, the curve at 60°C did not show hysteresis suggesting the absence of crevice corrosion even though the specimen was polarized up to 1 V SSC. At 90°C, the reverse scan showed a delayed hysteresis starting at approximately +500 mV SSC. Repassivation potential values are given in Table 2.

Figure 9 shows that in the 1 M NaF solution, both curves at 60°C and 90°C were free from hysteresis, suggesting the absence of crevice corrosion in pure fluoride solutions. At both temperatures, the polarization curves had the same characteristics (Figure 9). The highest polarization was approximately +800 mV SCC, suggesting that current flow (either by transpassive dissolution of by oxygen evolution) was easier in the 1 M NaF solutions (Figure 9) than in the 1 M NaCl solutions (Figure 8).

Figure 10 shows that the polarization curve at 60°C had an anodic peak in the passive region of potentials at approximately –30 mV SSC; however, at 90°C the curve did not exhibit the anodic peak. At 60°C, the polarization curve in the mixed halide solution did not have a hysteresis in the reverse scan suggesting the absence of crevice corrosion. In the 90°C solution, there was a delayed hysteresis starting at approximately +400 mV SSC.

Figures 11-12 show the polarization curves for Alloy 22 in the three studied electrolytes at 60°C and 90°C, respectively. The breakdown potentials were the highest in the NaCl solution and the lowest in the 1 M NaF solution (Figure 11). It is likely that current flow was easier when fluoride ions were present in the electrolyte because of the proper nature of fluoride or because the pH of the electrolyte was higher. In the reverse scan, the lowest potentials to reach a constant current of 1 μA/cm² (ER1) was for the mixed ion solution and the highest for the NaCl solution. Figure 12 shows that in the forward scan, the three polarization curves had a similar breakdown potential. In the reverse scan, the NaCl and the mixed solutions had a similar behavior. The reverse scan in the NaF solution occurred at the highest in potential.

Parameters from the Anodic Polarization Curves

In the cyclic potentiodynamic polarization (CPP) curves (Figures 8-12) there are several typical potentials. One of these potentials is the corrosion potential or the potential for which the applied cathodic and anodic currents are the same. Another typical potential is the breakdown potential for which the current density increases significantly and rather rapidly above the passive current density. The passive current density is defined as the region of potentials in which the current density is not highly dependent on the applied potential. In general, the CPP curves can be explained by extracting parameters from them, which would represent the breakdown and the repassivation potential behaviors. Table 2 shows the values of potential for which the current density reaches 20 μA/cm² and 200 μA/cm² in the forward scan and values of potential for which the current density reaches 10 μA/cm² and 1 μA/cm² in the reverse scan. The values of potential in the forward scan are called E20 and E200 and they represent potential breakdown values. Similarly, the two potentials in the reverse scan are called ER10 and ER1, which represent repassivation potential values (Table 2). [12-14,16] That is, in the forward scan, when the current density reaches for example 200 μA/cm² the passive behavior it can be considered that the of the alloy does not exist in the passive mode and that when the current density in the reverse scan has reached 1 μA/cm², the alloy has regained its passive behavior prior to the breakdown. Another parameter of interest is the repassivation potential determined as the intersection of the reverse scan with the forward scan. This is call ERCO or repassivation potential cross over (Table 2). [18] Table 2 shows that the value of ER1 to indicate total passivation is always available from a CPP curve, however ERCO values only exist when the intersection occurs, that is, in presence of hysteresis.

Figure 13 shows the breakdown potential E20 as a function of temperature for the three tested electrolytes. At 60°C, the highest average value of E20 was for the NaCl solution (pH ~ 6) and the lowest for the NaF solution (pH ~ 9). It is likely that at 60°C the behavior of E20 was mostly dictated by the pH of the electrolyte. At 90°C, the values of E20 for the three electrolytes are similar (Figure 13). It is likely that at the higher temperature there is an effect of both the pH and the nature of the halide on the value of E20. The effect of the temperature on the breakdown potential in the mixed halide solution had the same behavior as the breakdown potential in the pure chloride solution.

Figure 14 shows the repassivation potential ER1 as a function of the temperature for the three tested electrolytes. Both at 60°C and 90°C, the highest average value or ER1 was for the NaF solution, suggesting the absence of crevice corrosion in the pure fluoride solution under the tested conditions. The average value of ER1 in the NaCl solution decreased almost 400 mV between 60°C and 90°C suggesting a strong influence of the temperature on the susceptibility of Alloy 22 to crevice corrosion in NaCl solutions. The lowest repassivation potential both at 60°C and 90°C corresponded to the mixed halide

solution. Also, the dependence with the temperature of the repassivation potential values in the mixed halide had the same behavior as in the pure fluoride solution. ER1 values in NaF and in mixed halide were less dependent on the temperature than in NaCl solution.

Type of Attack in the Specimens after Anodic Polarization

In the 1 M NaCl solution at 60°C, the corrosion attack in the specimens after the CPP curve was only transpassive dissolution. The specimens were brown with some blue iridescent areas indicating high anodic polarizations (Figure 15). At 60°C, the specimens did not have crevice corrosion. The trapezoidal shapes outlined in Figure 15 (and subsequent figures) are result of the position of one of 24 crevice former teeth on the face of the specimens during testing. In 1 M NaCl solution at 90°C the specimens showed both transpassivity and typical crystalline crevice corrosion just underneath the crevice formers, in many cases outlining the entire perimeter of some of the 24 crevicing teeth in the crevice formers (Figure 16). Figure 16 shows less transpassive dissolution than Figure 15.

In the 1 M NaF solution at 60°C and 90°C, the corrosion attack in the specimens after the CPP curve was only transpassive dissolution (Figures 17 and 18). None of the tested specimens showed crevice corrosion. The boldly exposed areas of the specimens were gray-green and showed precipitation of salts or corrosion products, which were loosely adhered to the specimens. At 90°C (Figure 17), the outline of the crevice former teeth were better outlined on the specimen than at 60°C (Figure 18) but the specimen was still free from crevice corrosion.

In the 0.5 M NaCl + 0.5 M NaF solution at 60°C, the corrosion attack in the specimens after the CPP curve was mostly transpassive dissolution (Figure 19). However, at 60°C the specimens also showed a slight indication of crevice corrosion at this temperature, which was not evident in either the NaCl or NaF solutions at 60°C (Figures 15 and 17). [CC] There seems to be less transpassivity in the mixed halide solution at 60°C than in the pure chloride solution probably because less charge was circulated through the specimens (Figure 11). Also, since the pH of the mixed halide was lower than in the pure fluoride solution, less precipitation may have occurred (Figures 17 and 19). Figure 20 shows the aspect of a specimen tested in the mixed halide solution at 90°C. Abundant transpassivity with gray-green corrosion products and crystalline crevice corrosion is observed. The area of attack in the mixed halide solution (Figure 20) seemed similar to the area of attack in pure chloride solution (Figure 16).

The presence of fluoride ions in a chloride solution seems to increase the susceptibility of Alloy 22 to crevice corrosion. However a more detailed study is necessary to separate ions effect from pH effects. The three studied solutions reported here had slightly different pH values (from 6 to 9). A systematic study should be carried out by keeping the pH of the solution constant and by varying systematically the concentration of fluoride from trace amount (e.g. 10^{-3} M) to higher values in a more extended temperature range. It is also important to determine if the mode of crevice corrosion for Alloy 22, which was well established in pure chloride solutions [16] would change when in presence of fluoride (and bromide) ions.

[CC] It is common to observe in Alloy 22 two distinctive types of attack under the crevice formers when polarizing a specimen anodically. Type I of attack is obviously crevice corrosion since it manifests itself in a shiny crystalline mode. That is, the grains of the alloy are clearly discernible and even crystal planes within the grains are observable. In certain cases (sometimes depending on the mode the potential is applied or the type of tested material) the attack under the crevice former will appear as intergranular corrosion. On the other hand, Type II of attack has a spotty dull appearance that occurs under the crevice former but it is not different from the transpassive dissolution occurring in the boldly exposed surface of the specimen. In Type II attack, the environment under the crevice former does not seem to reach the aggressive conditions necessary for Type I attack (or crevice corrosion).

CONCLUSIONS

1. The 24-h E_{corr} of Alloy 22 was the highest in the 0.5 M NaCl + 0.5 M NaF pH 8 deaerated solution and the lowest in the 1 M NaF pH 9 deaerated solution. E_{corr} had an intermediate value in the 1 M NaCl pH 6 deaerated solution

2. The corrosion rate was the highest in the 1 M NaF solution and the lowest in the mixed halide solution.

3. Fluoride ions seem to act as a general corrosion inhibitor when added to a chloride solution

4. Using the CPP technique, Alloy 22 was resistant to crevice corrosion in 1 M NaCl solution at 60°C but was susceptible to crevice corrosion at 90°C

5. Alloy 22 was resistant to crevice corrosion in 1 M NaF both at 60°C and 90°C

6. Alloy 22 was slightly susceptible to crevice corrosion in the mixed halide solution at 60°C and susceptible at 90°C

7. The presence of fluoride ions in a chloride solution seems to increase the susceptibility of Alloy 22 to crevice corrosion

ACKNOWLEDGMENTS

This work was performed under the auspices of the U. S. Department of Energy (DOE) by the University of California Lawrence Livermore National Laboratory under contract N° W-7405-Eng-48. This work is supported by the Yucca Mountain Project, which is part of the Office of Civilian Radioactive Waste Management (OCRWM)

REFERENCES

1. ASTM International, Annual Book of ASTM Standards, Volume 02.04 “Non-Ferrous Metals” Standard 575 B (West Conshohocken, PA: ASTM International, 2002)
2. R. B. Rebak and P. Crook, Transportation, Storage and Disposal of Radioactive Materials, PVP-Vol. 483, p. 131 (American Society of Mechanical Engineers, 2004: New York, NY)
3. R. B. Rebak in Corrosion and Environmental Degradation, Volume II, p. 69 (Wiley-VCH, 2000: Weinheim, Germany)
4. R. B. Rebak and P. Crook, *Advanced Materials and Processes*, February 2000
5. R. B. Rebak and P. Crook, Proceeding of the Symposium Critical Factors in Localized Corrosion III, PV 98-17, p. 289 (The Electrochemical Society, 1998: Pennington, NJ)
6. D. C. Agarwal, Uhlig’s Corrosion Handbook, p. 831 (John Wiley & Sons, Inc., 2000: New York, NY)
7. E. L. Hibner and J. K. Patchell, Paper 04110, Corrosion/2004 (NACE International, 2004: Houston, TX)
8. K. A. Gruss, G. A. Cragnolino, D. S. Dunn and N. Sridhar, Paper 98149, Corrosion/1998 (NACE International, 1998: Houston, TX)
9. P. E. Manning, private communication (Haynes International, 2004: Kokomo, IN)

10. Yucca Mountain Science and Engineering Report, U. S. Department of Energy, Office of Civilian Radioactive Waste Management, DOE/RW-0539, Las Vegas, NV, May 2001
11. G. M. Gordon, Corrosion, 58, 811 (2002)
12. D. S. Dunn, L. Yang, Y.-M. Pan and G. A. Cragnolino, Paper 03697, Corrosion 2003 (NACE International, 2003: Houston, TX)
13. K. J. Evans, S. D. Day, G. O. Ilevbare, M. T. Whalen, K. J. King, G. A. Hust, L. L. Wong, J. C. Estill and R. B. Rebak, Transportation, Storage and Disposal of Radioactive Materials, PVP-Vol. 467, p. 55 (American Society of Mechanical Engineers, 2003: New York, NY)
14. K. J. Evans, A. Yilmaz, S. D. Day, L. L. Wong, J. C. Estill and R. B. Rebak "Comparison of Electrochemical Methods to Determine Crevice Corrosion Repassivation Potential of Alloy 22 in Chloride Solutions," JOM, January 2005 (TMS, 2005: Warrendale, PA)
15. D. S. Dunn and C. S. Brossia, Paper 02548, Corrosion 2002 (NACE International, 2002: Houston, TX)
16. K. J. Evans, L. L. Wong and R. B. Rebak, Transportation, Storage and Disposal of Radioactive Materials, PVP-Vol. 483, p. 137 (American Society of Mechanical Engineers, 2004: New York, NY)
17. G. O. Ilevbare, K. J. King, S. R. Gordon, H. A. Elayat, G. E. Gdowski and T. S. E. Summers "Effect of Nitrate on the Repassivation Potential of Alloy 22 in Chloride Containing Solutions," Fall 2004 Meeting of the Electrochemical Society, 0308Oct04, Honolulu, HI (to be published)
18. J. H. Lee, T. Summers and R. B. Rebak, Paper 04692, Corrosion/2004 (NACE International, 2004: Houston, TX)
19. B. A. Kehler, G. O. Ilevbare and J. C. Scully, Corrosion, p. 1042 (2001)
20. K. J. Evans and R. B. Rebak, PV 2002-13, p. 344 (The Electrochemical Society, 2002: Pennington, NJ)
21. G. A. Cragnolino, D. S. Dunn and Y.-M. Pan "Localized Corrosion Susceptibility of Alloy 22 as a Waste Package Container Material," Scientific Basis for Nuclear Waste Management XXV, Vol. 713, p. 53 (Materials Research Society 2002: Warrendale, PA)
22. D. S. Dunn, L. Yang, C. Wu and G. A. Cragnolino, Mat. Res. Soc. Symp. Proc. Vol 824 (MRS, 2004: Warrendale, PA)
23. D. S. Dunn, Y.-M. Pan, K. Chiang, L. Yang, G. A. Cragnolino and X. He "Localized Corrosion Resistance and Mechanical Properties of Alloy 22 Waste Package Outer Containers" JOM, January 2005 (TMS, 2005: Warrendale, PA)
24. G. O. Ilevbare, "The Effect of Sulfate Anions on the Crevice Corrosion in Alloy 22" (Submitted for publication to Corrosion Journal)
25. N. S. Meck, P. Crook, S. D. Day and R. B. Rebak, Paper 03682, Corrosion/2003 (NACE International, 2003: Houston, TX)
26. M. A. Rodríguez, R. M. Carranza and R. B. Rebak, Paper 04700, Corrosion/2004 (NACE International, 2004: Houston, TX)
27. M. A. Rodríguez, R. M. Carranza and R. B. Rebak, "Influence of Halide Ions and Alloy Microstructure on the Passive and Localized Corrosion Behavior of Alloy 22," Met. Trans. A (to be published)
28. R. B. Rebak, N. E. Koon, J. P. Cotner and P. Crook, ECS PV 99-27, p. 473 (The Electrochemical Society, 1999: Pennington, NJ)
29. R. B. Rebak, Paper 05610, Corrosion/2005 (NACE International, 2005: Houston, TX)
30. ASTM International, Annual Book of ASTM Standards, Volume 03.02 "Wear and Erosion; Metal Corrosion" G-15, G-61, etc. (West Conshohocken, PA: ASTM International, 2004)
31. J. C. Estill, G. A. Hust and R. B. Rebak, Paper 03688, Corrosion/2003 (NACE International, 2003: Houston, TX)

TABLE 1
CHEMICAL COMPOSITION IN WEIGHT % OF THE TESTED SPECIMENS
ALL SPECIMENS WROUGHT MILL ANNEALED

Specimens/Element	Ni	Cr	Mo	W	Fe	Others
Nominal ASTM B 575	50-62	20-22.5	12.5-14.5	2.5-3.5	2-6	2.5Co-0.5Mn-0.35V (A)
DEA3129-DEA3271 Heat 2277-1-3265	~57	21.2	12.9	2.5-3.5	3.9	0.7Co-0.25Mn-0.17V
SRG01 and SRG13 Heat 059902LL1	59.56	20.38	13.82	2.64	2.85	0.17V-0.16Mn

(A) Maximum

TABLE 2
CHARACTERISTIC POTENTIALS (mV, SSC) AND CORROSION RATES FOR ALLOY 22

Specimen ID	24-h $E_{corr,}$	Corrosion Rate (μm/year)	E20	E200	ER10	ER1	ERCO
	1 M NaCl, 60°C						
DEA3147 (A)	-428	0.77, 0.70, 0.58	638	805	685	132	163
DEA3148 (A)	-426	0.75, 0.87, 0.83	663	802	689	598	NA
DEA3267 (A)	-369	0.14, 0.15, 0.17	604	816	670	62	44
DEA3268 (A)	-421	0.52, 0.58, 0.67	600	816	665	27	15
DEA3273 (A)	-458	0.13, 0.05, 0.15	570	813	683	578	NA
DEA3264	-429	0.27, 0.33, 0.31	606	781	672	551	NA
DEA3265	-520	1.55, 1.17, 1.27	634	766	667	552	NA
	1 M NaCl, 90°C						
SRG01 (B)	-578	1.23, 1, 0.62	302	527	-9	-72	-79
SRG13 (B)	-577	1.69, 1.53, 1.29	306	513	-6	-76	-80
DEA3129	-298	0.74, 0.95, 0.63	234	674	25	-51	-24
DEA3130	-237	0.93, 1.2, 0.68	291	582	-14	-75	-67
DEA3262	-571	1.93, 1.66, 1.36	386	635	30	-94	-53
DEA3263	-599	2.55, 2.40, 1.29	315	612	20	-99	-54
DEA3269 (A)	-548	1.21, 1.04, 0.61	271	631	-10	-66	-66
DEA3271 (A)	-457	0.41, 0.51, 0.23	378	524	11	-59	-44
	1 M NaF, 60°C						
DEA3155	-623	0.37, 0.27, 0.086	406	523	435	339	NA
DEA3156	-642	1.21, 1.07, 0.138	403	516	435	343	NA
	1 M NaF, 90°C						
DEA3153	-661	3.05, 2.18, 1.70	369	688	435	271	534 (C)
DEA3154	-657	2.33, 2.27, 1.06	195	674	391	173	522 (C)
	0.5 M NaCl + 0.5 M NaF, 60°C						
DEA3149	-252	0.39, 0.38, 0.39	522	570	414	0	168
DEA3150	-389	0.17, 0.18, 0.16	500	582	496	140	NA
	0.5 M NaCl + 0.5 M NaF, 90°C						
DEA3151	-477	0.30, 0.84, 0.53	163	544	94	-91	-42
DEA3152	-522	0.27, 0.60, 0.77	314	542	80	-104	-114

E20 and E200 are the potentials in the forward scan of a CPP curve for which the current densities reach 20 μA/cm² and 200 μA/cm², respectively. ER10 and ER1 are the potentials for which the current density in the reverse scan reaches 10 μA/cm² and 1 μA/cm², respectively. ERCO is the potential at which the reverse scan crosses over the forward scan. (A) 1.25 M NaCl, NA = Not Available or Not Applicable, (B) PCA specimen (Prism Crevice Assembly), (C) Cross over in the transpassive region of potentials

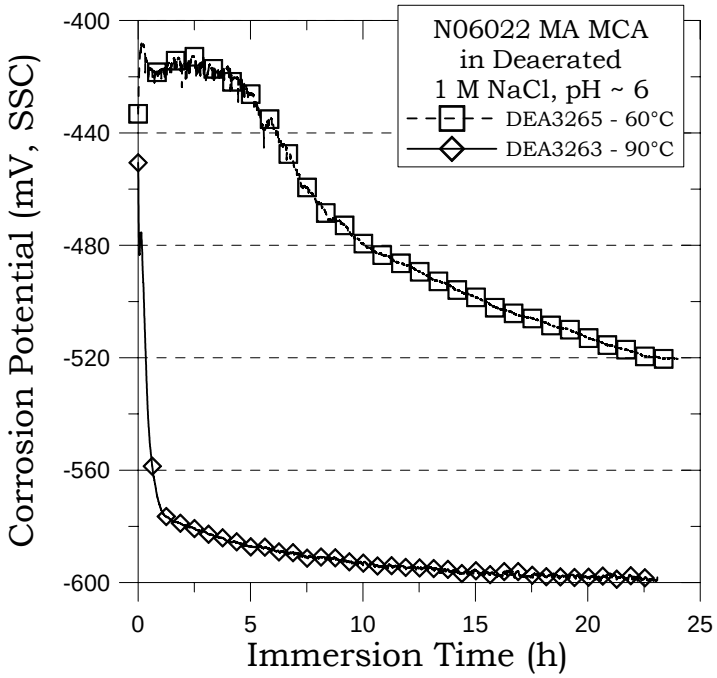

FIGURE 1 – E_{corr} as a function of time for Alloy 22 Specimens in 1 M NaCl

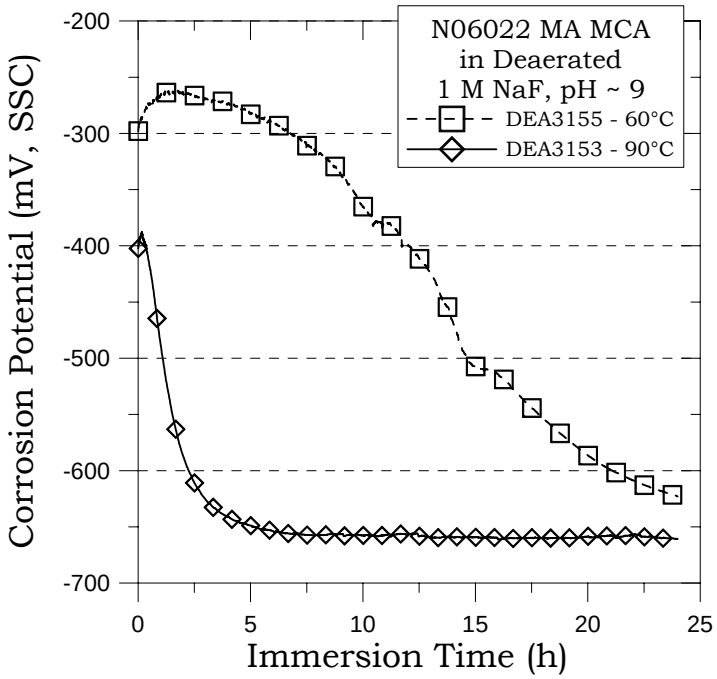

FIGURE 2 – E_{corr} as a function of time for Alloy 22 Specimens in 1 M NaF

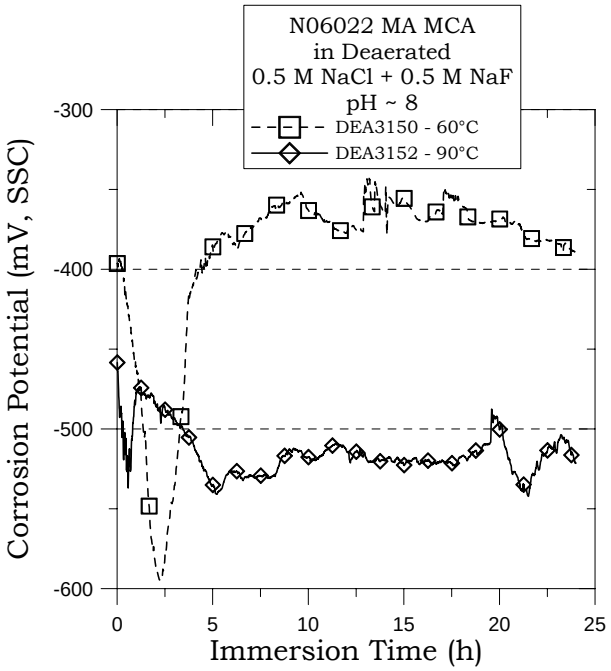

FIGURE 3 – E_{corr} as a function of time for Alloy 22 Specimens in 0.5 M NaCl + 0.5 M NaF

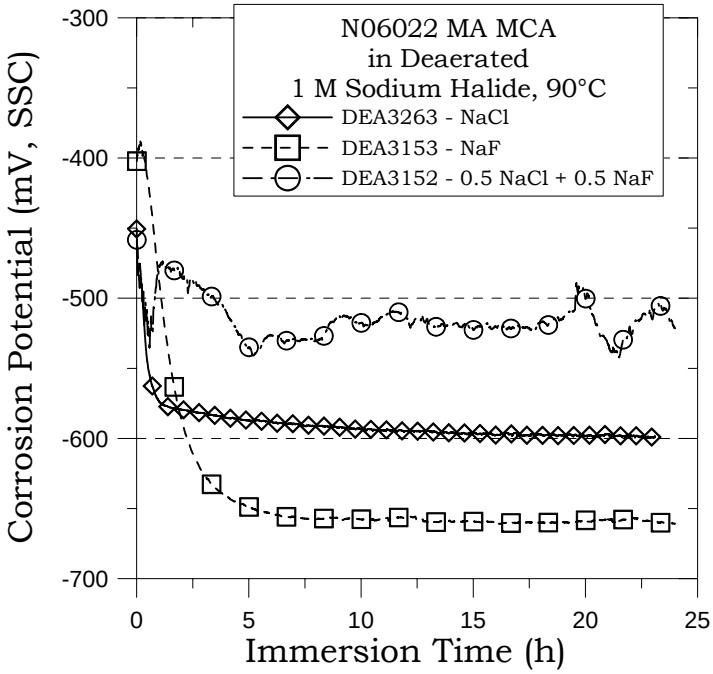

FIGURE 4 – E_{corr} as a function of time for Alloy 22 Specimens in 1 M Halide at 90°C

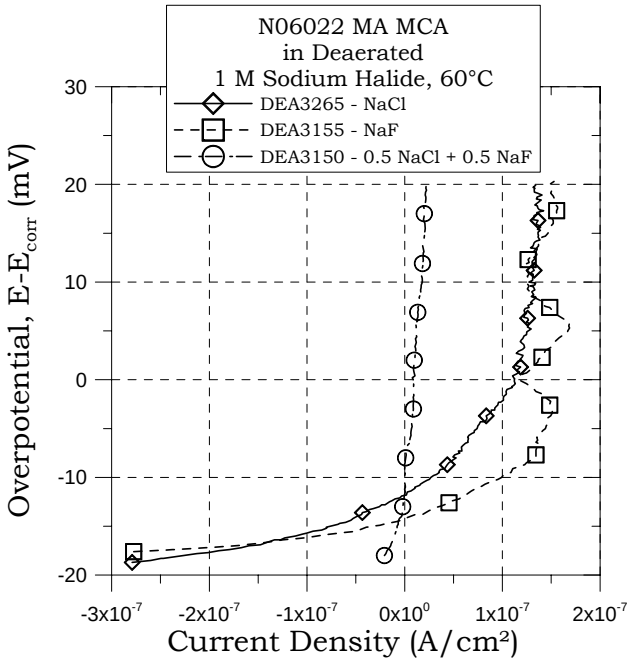

FIGURE 5 – Resistance to Polarization for Alloy 22 in 1 M Halide at 60°C

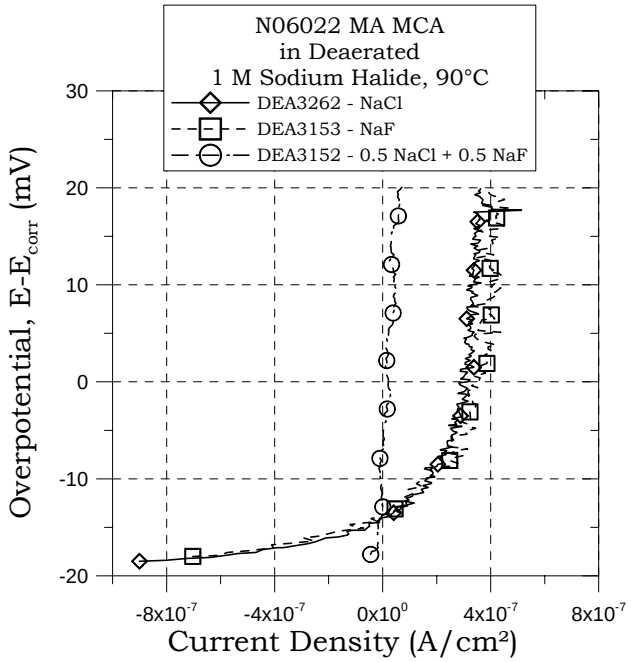

FIGURE 6 – Resistance to Polarization for Alloy 22 in 1 M Halide at 90°C

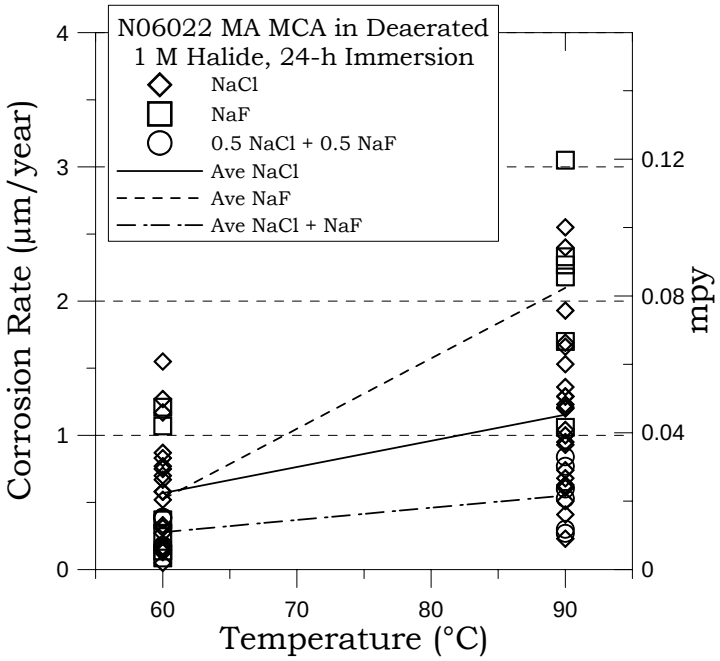

FIGURE 7 – Average Corrosion Rate for Alloy 22 in 1 M Halide as a function of temperature

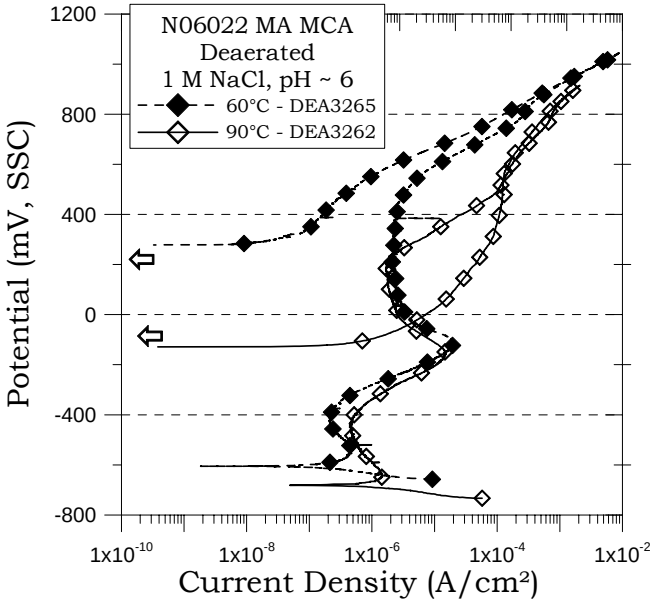

FIGURE 8 – CPP curves for Alloy 22 in 1 M NaCl solution at 60°C and 90ºC

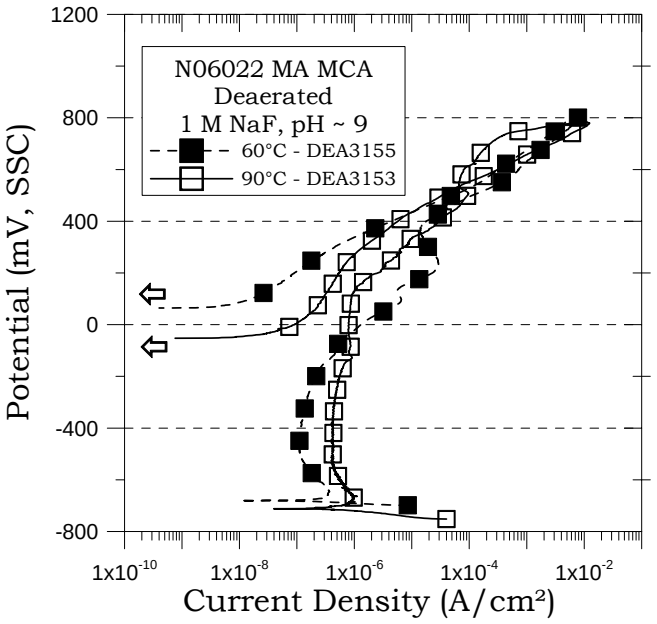

FIGURE 9 – CPP curves for Alloy 22 in 1 M NaF solution at 60°C and 90ºC

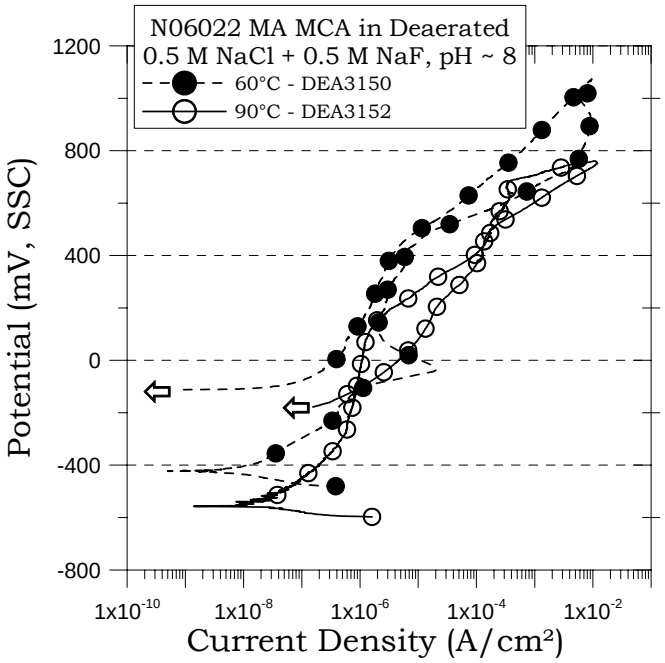

FIGURE 10 – CPP curves for Alloy 22 in 0.5 M NaCl + 0.5 M NaF solution at 60°C and 90ºC

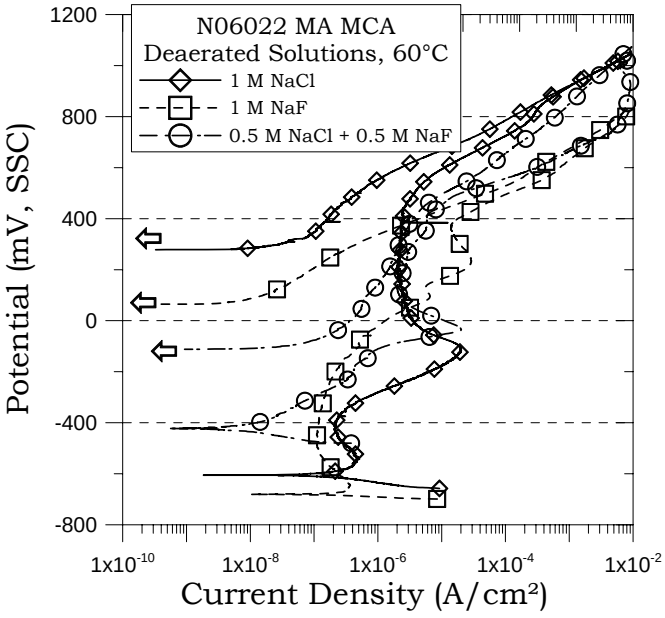

FIGURE 11 – CPP curves for Alloy 22 in 1 M Halide solutions at 60°C

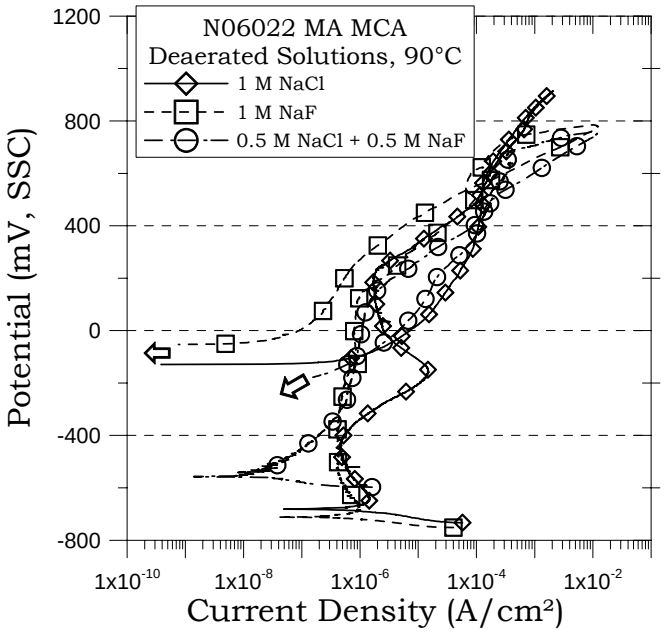

FIGURE 12 – CPP curves for Alloy 22 in 1 M Halide solutions at 90°C

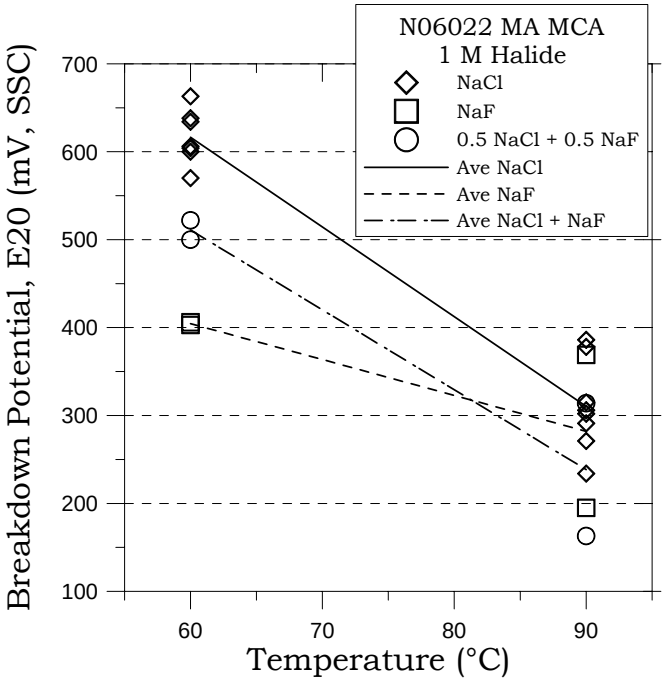

FIGURE 13 – Breakdown Potential E20 for Alloy 22 in the three halide solutions

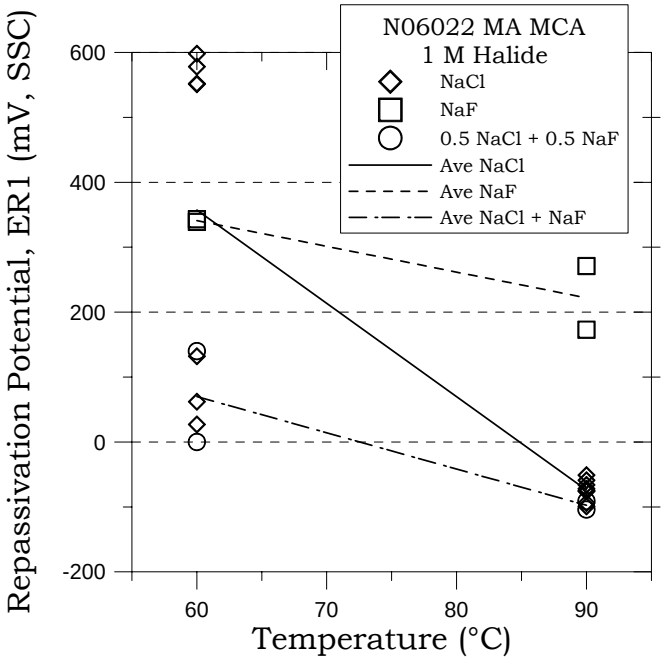

FIGURE 14 – Repassivation Potential ER1 for Alloy 22 in the three halide solutions

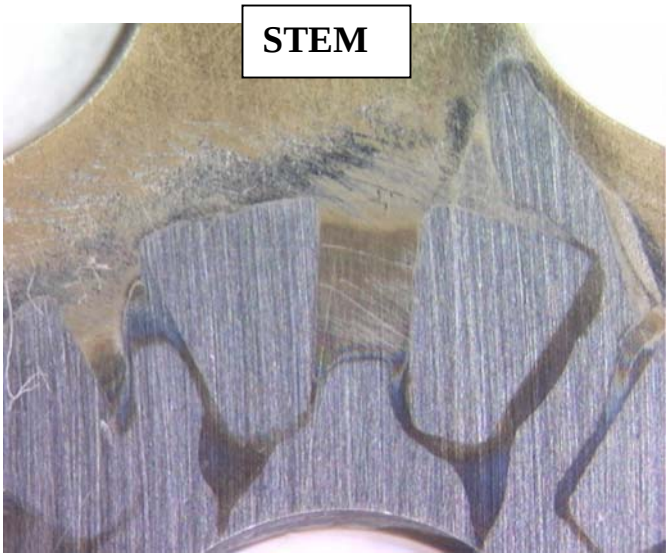

FIGURE 15 – Specimen DEA3264 after CPP in 1 M NaCl at 60°C. The top section of the creviced round part of the lollipop (MCA) specimen is shown. Brown-blue transpassive dissolution. The specimen is free from crevice corrosion. Magnification X ~10.

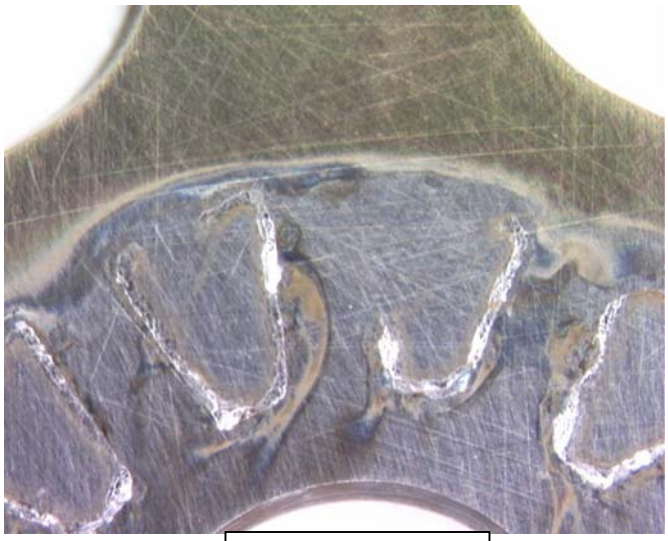

FIGURE 16 – Specimen DEA3262 after CPP in 1 M NaCl at 90°C. Transpassive dissolution and crystalline crevice corrosion. Magnification X ~10

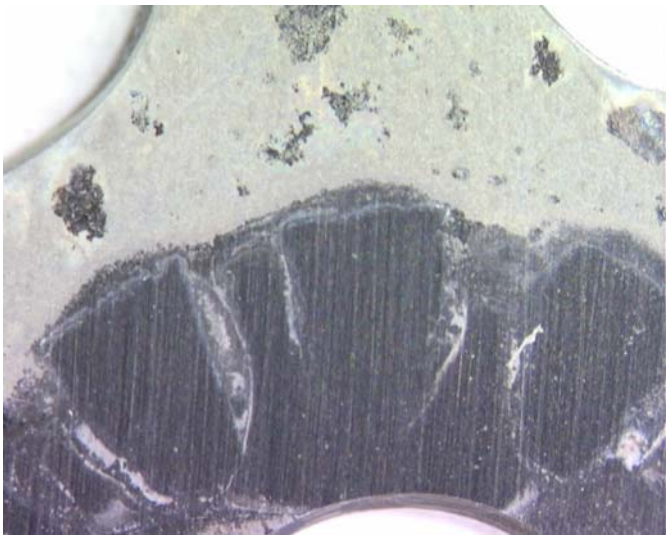

FIGURE 17 – Specimen DEA3156 after CPP in 1 M NaF at 60°C. Only transpassive dissolution. The specimen is free from crevice corrosion. Magnification X ~10

FIGURE 18 – Specimen DEA3153 after CPP in 1 M NaF at 90°C. Only transpassive dissolution. The specimen is free from crevice corrosion. Magnification X ~10.

FIGURE 19 – Specimen DEA3150 after CPP in 0.5 M NaCl + 0.5 M NaF at 60°C. Transpassive dissolution and traces of crevice corrosion. Magnification X ~10.

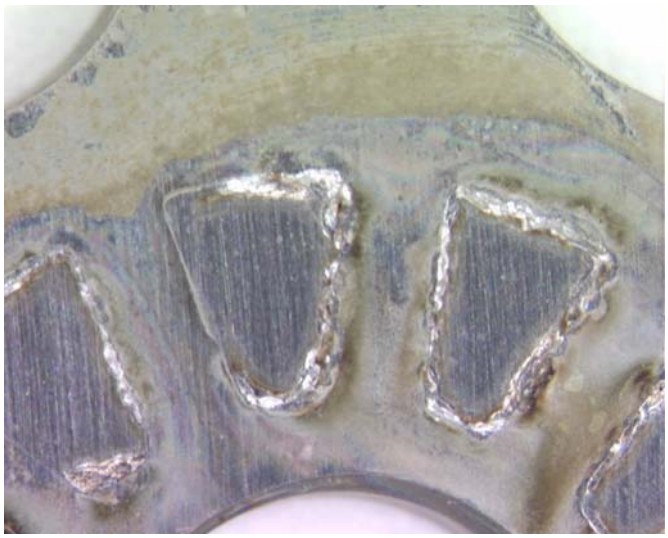

FIGURE 20 – Specimen DEA3264 after CPP in 0.5 M NaCl + 0.5 M NaF at 90°C. Abundant transpassive dissolution and crystalline crevice corrosion. Magnification X ~10.